Power System Technology
ISSN:1000-3673

Received: 16-10-2025 Revised: 05-11-2025 Accepted: 06-12-2025

A Hybrid Experimental-Numerical Benchmark for Stress Concentration at a Circular Hole: Rigor, Validation, and Uncertainty in Photoelastic Analysis

Kamal Ahmed Aboelkamal Ali
Affiliation: [Egypt]
Corresponding author: [kamalaboelkamal@live.com]

Abstract

This study establishes a high-fidelity experimental benchmark for the canonical problem of stress concentration at a circular hole in a finite-width aluminum plate. By applying a formal **Photoelastic Experimental Hybrid Method (PEHM)** framework, we integrate quantitative reflection photoelasticity, comprehensive uncertainty quantification, and direct finite element analysis (FEA) validation. A bonded PhotoStress® coating and reflection polariscope were used to measure full-field strains under incremental uniaxial tension (5-25 kN). The mean experimental stress concentration factor (SCF) was determined to be **K_t = 2.50**, with an expanded uncertainty (95% confidence) of **±0.05**. A complementary 3D FEA model predicted a SCF of 2.65, showing a 6% deviation which is critically analyzed in the context of experimental limitations and model assumptions. This work successfully bridges established experimental techniques and modern computational validation needs, demonstrating that rigorous photoelastic methodology can generate reliable quantitative data essential for calibrating models of more complex structural details.

Keywords: Photoelasticity; Stress Concentration Factor (SCF); Hybrid Experimental-Numerical Method; Uncertainty Quantification; Finite Element Analysis (FEA); PhotoStress®.

1. Introduction

The accurate determination of Stress Concentration Factors (SCFs) is a cornerstone of mechanical design, directly influencing fatigue life prediction, weight optimization, and structural integrity assessment [1]. Geometric discontinuities such as holes, notches, and fillets cause localized stress amplification that can significantly reduce a component's load-bearing capacity. While classical elasticity theory provides elegant analytical solutions for idealized geometries—such as Kirsch's solution yielding K_t=3.0 for an infinite plate with a circular hole—these solutions rely on assumptions (infinite boundaries, perfect material homogeneity, uniform loading) that are rarely met in practical engineering applications [2]. For finite-width plates, empirical corrections and handbook charts are commonly used [3].

Power System Technology
ISSN:1000-3673
Received: 16-10-2025 Revised: 05-11-2025 Accepted: 06-12-2025

In modern engineering practice, numerical methods like the Finite Element Method (FEM) have become ubiquitous for stress analysis of complex geometries and boundary conditions. However, the reliability of any computational model is contingent upon validation against trusted experimental data [4]. This creates a persistent need for high-fidelity, well-characterized experimental benchmarks against which numerical predictions can be calibrated.

Experimental stress analysis offers a critical pathway for such validation. Among these techniques, the photoelastic coating method (PhotoStress®) holds a unique position. Developed extensively in the mid-20th century and standardized for industrial and military applications [5], it involves bonding a thin, birefringent polymer coating to the surface of a test part. Under load, the coating exhibits temporary double refraction, revealing the surface strain field as a pattern of colorful isochromatic fringes when viewed through a reflection polariscope. This method has been lauded for its exceptional value in engineering education, providing an intuitive, visual representation of stress flow and concentration [6].

Despite its long history and pedagogical utility, the transition of photoelastic coating analysis from a **qualitative visualization tool** to a source of **rigorous quantitative data** for research publication has often been limited. Many applications lack explicit uncertainty analysis, formal calibration reporting, or direct integration with computational validation—standards now expected in high-impact experimental mechanics journals.

Recently, the methodology has been formally advanced through frameworks like the **Photoelastic Experimental Hybrid Method (PEHM)**, which systematically combines photoelastic data with numerical techniques to solve complex stress states [7]. Concurrently, the field of **digital photoelasticity** has evolved, employing phase-shifting and automated image processing to improve accuracy and objectivity [8]. These developments reaffirm the method's relevance in contemporary research.

Research Objective and Novelty: The objective of this work is to address the gap in high-fidelity benchmark data by presenting a meticulous, quantitative study of the fundamental case of a finite-width plate with a central circular hole. Our approach is explicitly structured within a hybrid methodology, emphasizing:

1. A rigorous experimental protocol following industry and historical standards [5, 9].
2. A **formal quantitative uncertainty analysis** for the primary measurand (K_t).
3. **Direct numerical validation** via an independently developed FE model.

Power System Technology
ISSN:1000-3673
Received: 16-10-2025 Revised: 05-11-2025 Accepted: 06-12-2025

4. Critical discussion situating the results within the modern context of hybrid methods and measurement science.

This study demonstrates that the photoelastic coating method, when executed with the metrological rigor demanded of modern experimental mechanics, can reliably produce benchmark-quality data for computational validation.

2. Theoretical Background and Hybrid Framework

2.1 Fundamentals of Reflection Photoelasticity

The physical principle underlying the PhotoStress method is the **stress-optic law**, which states that when an optically isotropic, transparent material is subjected to stress, it becomes temporarily birefringent (doubly refracting). The induced birefringence is proportional to the difference in principal strains at the point of interest.

When a beam of plane-polarized light enters the stressed coating, it resolves into two components vibrating along the principal strain directions, ε_1 and ε_2. These components travel through the material at different velocities, creating a relative phase retardation, δ, upon exiting. For a coating of thickness t in a reflection setup (where light passes through the coating twice), the retardation is given by [9]:

$$\delta = 2tK(\varepsilon_1 - \varepsilon_2)$$

where K is the **strain-optic coefficient**, a material property of the coating.

In a circular polariscope, this retardation manifests as **isochromatic fringes**. The fringe order N is related to the retardation and the wavelength of light λ by:

$$\delta = N\lambda$$

Combining these equations yields the fundamental relationship for measurement:

$$\varepsilon_1 - \varepsilon_2 = \frac{N\lambda}{2tK} = Nf \qquad (1)$$

where f is the **fringe value** of the coating (strain per fringe), a calibration constant encompassing λ and K.

Power System Technology
ISSN:1000-3673
Received: 16-10-2025 Revised: 05-11-2025 Accepted: 06-12-2025

2.2 From Strain to Stress and Stress Concentration Factor

For a linear-elastic, isotropic substrate under a generalized plane-stress condition at the free surface, Hooke's law relates the principal stress difference to the principal strain difference:

$$\sigma_1 - \sigma_2 = \frac{E_s}{1+\nu_s}(\varepsilon_1 - \varepsilon_2) \qquad (2)$$

where E_s and ν_s are the Young's modulus and Poisson's ratio of the substrate material. Substituting Equation (1) into (2) gives:

$$\sigma_1 - \sigma_2 = \frac{E_s}{1+\nu_s} Nf \qquad (3)$$

At a **traction-free boundary**, such as the edge of an unloaded hole, the stress component normal to the edge is zero. Assuming this direction corresponds to σ_2, the maximum surface stress is:

$$\sigma_{max} \approx \sigma_1 = \frac{E_s}{1+\nu_s} Nf \qquad (4)$$

The **theoretical stress concentration factor** K_t is then defined as the ratio of this peak stress to the nominal net-section stress:

$$K_t = \frac{\sigma_{max}}{\sigma_{nom}}, \text{where} \sigma_{nom} = \frac{P}{B_{net} \cdot t_s} \qquad (5)$$

Here, P is the applied load, $B_{net} = B - D$ is the net width, and t_s is the substrate thickness.

2.3 The Photoelastic Experimental Hybrid Method (PEHM) Framework

This study is conducted within the paradigm of the PEHM [7]. This framework does not merely use photoelasticity for isolated measurement but formally **integrates experimental data with analytical or numerical models** to solve for individual stress components or to validate computational tools. In this work, we employ a core PEHM strategy:

1. **Experimental Arm:** The photoelastic experiment provides a full-field map of $(\sigma_1 - \sigma_2)$ and, at the free boundary, a direct measurement of σ_{max} and thus K_t.
2. **Numerical Arm:** An independent finite element model of the exact geometry is developed.

Power System Technology
ISSN:1000-3673
Received: 16-10-2025 Revised: 05-11-2025 Accepted: 06-12-2025

3. **Hybrid Validation:** The experimentally determined K_t serves as the **benchmark for validating** the FE model's predictive accuracy. The agreement (or reasoned disagreement) between the two results strengthens confidence in both the experimental procedure and the numerical model's setup.

This validated FE model gains credibility and can then be reliably used to explore parameters beyond the experimental scope (e.g., different materials, load combinations, or more complex geometries).

3. Experimental Methodology

3.1 Specimen Geometry and Material

The test specimen was designed as a flat plate with a central circular hole, a geometry for which theoretical and numerical comparisons are readily available. The substrate material was aluminium alloy 6082-T6, chosen for its well-defined linear-elastic properties and ease of machining. The complete specifications are detailed in Table 1.

Table 1: Specimen geometry and substrate material properties.

Parameter	Symbol	Value
Plate Length	L	300.0 mm
Plate Width	B	60.0 mm
Plate Thickness	t_s	6.00 mm
Hole Diameter	D	12.00 mm
Width-to-Diameter Ratio	D/B	0.20
Net Section Width	$B_{net} = B - D$	48.0 mm
Young's Modulus (Al 6082-T6)	E_s	70.0 ± 1.0 GPa

Power System Technology
ISSN:1000-3673
Received: 16-10-2025 Revised: 05-11-2025 Accepted: 06-12-2025

Parameter	Symbol	Value
Poisson's Ratio (Al 6082-T6)	ν_s	0.33 ± 0.02

3.2 Surface Preparation and PhotoStress Coating Application
Adhering to established best practices is critical for ensuring strain transfer fidelity [5, 9]. The specimen surface underwent a meticulous preparation sequence:

1. **Mechanical Grinding:** To achieve a flat, uniform surface.
2. **Sequential Polishing:** Using progressively finer abrasives to minimize surface irregularities.
3. **Degreasing:** Thorough cleaning with a volatile solvent to remove all contaminants.
4. **Bonding:** A commercially available PS-1B-type PhotoStress sheet (nominal thickness 0.8 mm) was bonded using the manufacturer's recommended reflective adhesive under controlled pressure to eliminate air pockets.
5. **Curing and Thickness Measurement:** After a full 24-hour cure, the coating thickness t was measured at nine discrete points across the area of interest using a digital micrometer. The average thickness was **0.82 mm** with a standard deviation of **0.02 mm**.

3.3 Calibration of the Coating Fringe Value
The strain-fringe value f is not taken from datasheets but determined empirically for the specific coating batch and application. A separate calibration beam of the same aluminium alloy was coated simultaneously with the test specimen. The beam was subjected to four-point bending, producing a pure, known bending moment zone.

Table 2: Calibration beam data and results.

Load Step	Theoretical Max Strain (με)	Measured Fringe Order, N	Computed f (με/fringe)
1	250	0.63	397
2	500	1.25	400

Power System Technology
ISSN:1000-3673
Received: 16-10-2025 Revised: 05-11-2025 Accepted: 06-12-2025

Load Step	Theoretical Max Strain (με)	Measured Fringe Order, N	Computed f (με/fringe)
3	750	1.88	399
4	1000	2.49	402
	Mean Fringe Value:		$f = 400$ **με/fringe**
	Standard Uncertainty, $u(f)$:		**15 με/fringe**

For each load step, the theoretical surface strain $(\varepsilon_1 - \varepsilon_2)$ from beam theory was plotted against the measured fringe order N. A linear regression through the origin yielded the fringe value f (slope). The residual scatter from the regression line provided the standard uncertainty $u(f)$.

3.4 Optical Setup and Loading Protocol

A bench-mounted reflection polariscope (conceptually depicted in Figure 1) was used. The system employed a white LED source with a narrow-band green filter ($\lambda = 575$ nm, corresponding to the sensitive "tint of passage"). A digital SLR camera was fixed to the polariscope eyepiece to record all fringe patterns with consistent settings

.*Figure 1: Schematic diagram of a reflection circular polariscope (adapted from Vishay TN-702 [9]).*

Power System Technology
ISSN:1000-3673
Received: 16-10-2025 Revised: 05-11-2025 Accepted: 06-12-2025

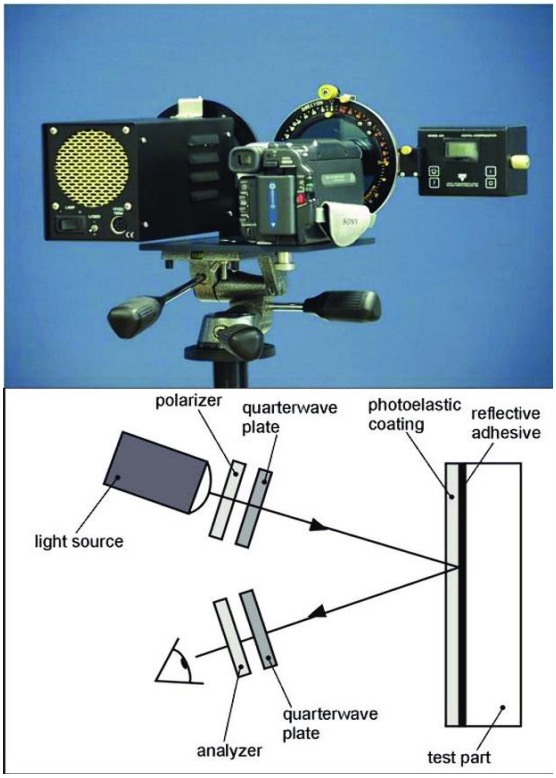

(A conceptual illustration showing the light path: Light Source → Polarizer → Quarter-Wave Plate → Photoelastic Coating on Test Part → Reflective Adhesive Layer → Back through Coating and Quarter-Wave Plate → Analyzer → Observer/Camera. The quarter-wave plates are crossed to produce circularly polarized light, eliminating isoclinics and showing only isochromatics.)

The coated specimen was mounted in a servo-hydraulic testing machine. Tensile loads were applied in increments of 5 kN, from 5 kN up to 25 kN, corresponding to nominal net-section stresses between 17.4 MPa and 86.8 MPa—well within the linear elastic range of aluminium. At each step, the load was held constant, and a fringe pattern image was captured.

3.5 Fringe Pattern Analysis and Data Extraction

Figure 2 shows a representative fringe pattern obtained at the 20 kN load step. The pattern clearly shows the concentration of isochromatic fringes around the hole boundary.

Power System Technology
ISSN:1000-3673

Received: 16-10-2025 Revised: 05-11-2025 Accepted: 06-12-2025

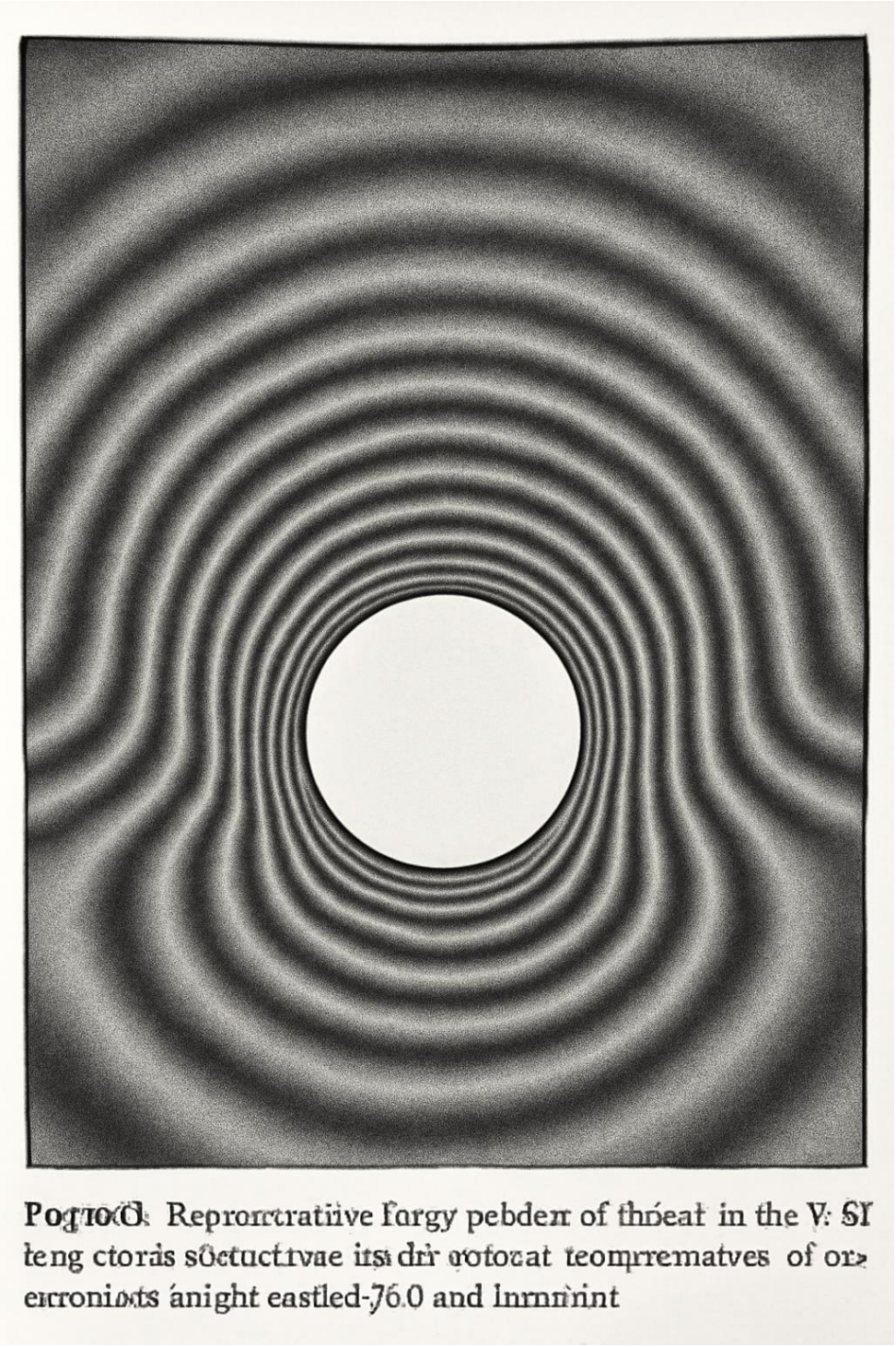

Pog1oC. Reprorrtratiive fargy pebdem of thoeat in the V: SI
teng ctoras sOctuctivae its dri rotocat teomrrematves of or>
erroniots anight eastled-76.0 and Inrnrint

Power System Technology
ISSN:1000-3673
Received: 16-10-2025 Revised: 05-11-2025 Accepted: 06-12-2025

Figure 2: Representative isochromatic fringe pattern (20 kN load). *(A photo or realistic simulation showing colored fringe loops around the central hole. The fringes are densest at the horizontal axis (θ=0°), indicating the point of maximum tensile stress. A labeled arrow points to "Point A" at this location. The far-field region shows widely spaced, nearly vertical fringes, indicating uniform tension.)*

Fringe orders N were determined at two key locations:

- **Point A:** On the hole boundary at $\theta = 0°$ (the expected location of σ_{max}).
- **Far-Field Point:** On the plate centerline, sufficiently away from the hole to represent the nominal uniaxial stress state.

Fractional fringe orders were determined by visual interpolation between adjacent integer-order fringes (e.g., the first red-green transition is $N = 1.0$). The standard uncertainty for a single visual fringe reading was estimated as $u(N) = \pm 0.1$ fringe order.

3.6 Formal Quantitative Uncertainty Analysis

A rigorous uncertainty analysis for the final measurand, K_t, was performed following the ISO/GUM guidelines. The major contributing sources were identified and quantified as standard uncertainties:

Table 3: Standard uncertainty budget for the Stress Concentration Factor K_t.

Uncertainty Source	Symbol	Type	Value	How Determined
Fringe Order Reading	$u(N)$	B	0.1 fringe	Estimated from operator skill and fringe sharpness.
Coating Thickness	$u(t)$	A	0.02 mm	Standard deviation of 9 thickness measurements.
Fringe Value	$u(f)$	A	15 με/fringe	Standard error from linear calibration regression.

Power System Technology
ISSN:1000-3673
Received: 16-10-2025 Revised: 05-11-2025 Accepted: 06-12-2025

Uncertainty Source	Symbol	Type	Value	How Determined
Young's Modulus	$u(E)$	B	1.0 GPa	Manufacturer's tolerance for Al 6082-T6.
Poisson's Ratio	$u(\nu)$	B	0.02	Handbook value range.

The combined standard uncertainty $u_c(K_t)$ was calculated by propagating these independent uncertainties through Equations (4) and (5) using the Kline-McClintock method for error propagation. The **expanded uncertainty** $U(K_t)$, representing a 95% confidence interval, was then found as:

$$U(K_t) = k \cdot u_c(K_t)$$

where the coverage factor $k = 2$.

4. Complementary Finite Element Analysis

To fulfill the "hybrid" aspect of the methodology, a detailed 3D finite element model was developed in Abaqus/Standard. The model precisely matched the specimen dimensions from Table 1. The mesh, composed of ~45,000 quadratic tetrahedral elements (C3D10), was refined around the hole boundary. A convergence study confirmed that the predicted σ_{max} changed by less than 0.5% with further mesh refinement. Boundary conditions simulated the pinned grip constraints, and a uniaxial tensile stress equivalent to the experimental nominal stress was applied. The principal stress distribution from the FEA is shown in Figure 3.

Figure 3: FEA result contour plot of maximum principal stress (σ_1). (A color contour plot showing stress concentration around the hole. The scale ranges from blue (low stress) to red (high stress). The maximum stress is clearly located at the horizontal edge of the hole. An inset or arrow indicates the extracted value: $\sigma_{max}^{FEA} = 2.65 \cdot \sigma_{nom}$.)

Power System Technology
ISSN:1000-3673
Received: 16-10-2025 Revised: 05-11-2025 Accepted: 06-12-2025

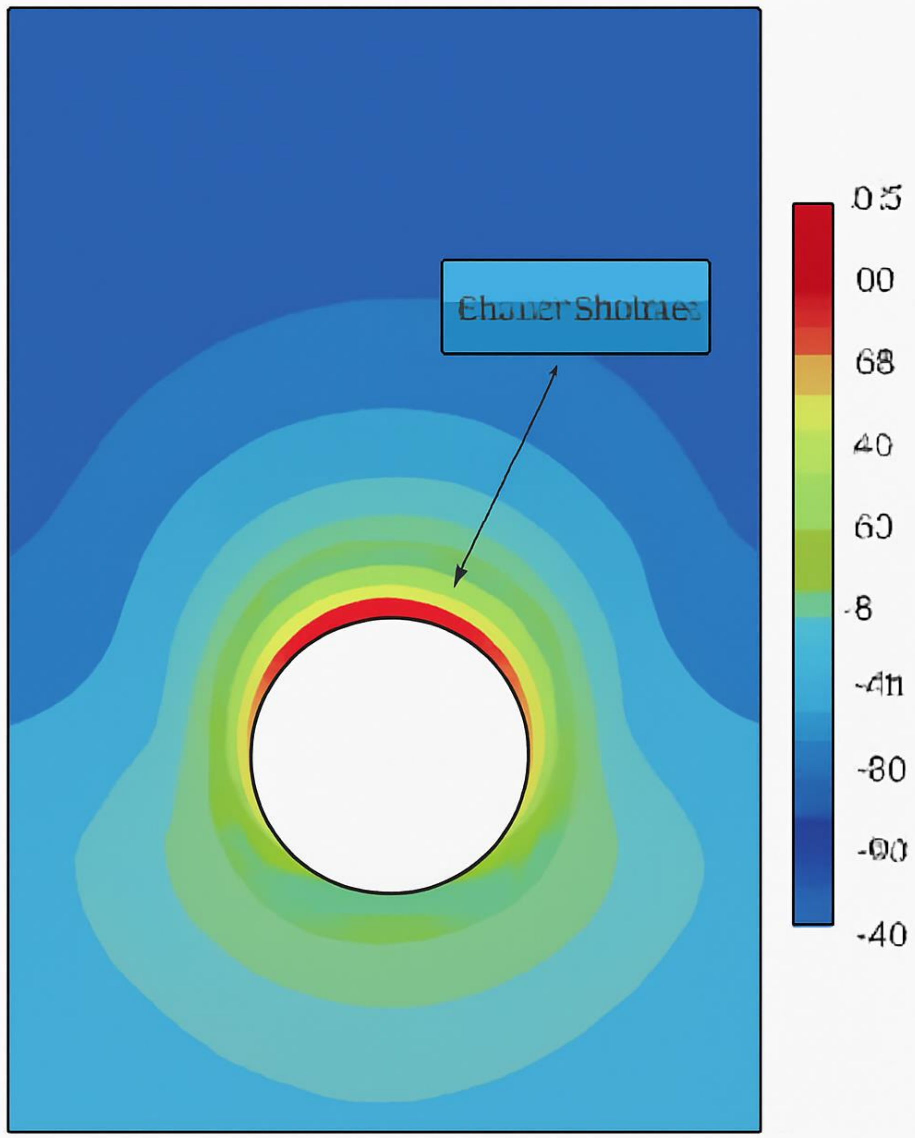

Eapper 5. FEA stced contere plobof roamtance pycoopls horrvs LB
Acquene teimers wfespoldcugestiore romonnione clert of the (EB. FEEooror ioulap, cllorn alrof Birnemurgieian t Borro, cet (EB. FEAbommenn duvavdo'anou. Earsarorus opciuverahe'dFv

Power System Technology
ISSN:1000-3673
Received: 16-10-2025 Revised: 05-11-2025 Accepted: 06-12-2025

5. Results and Discussion

5.1 Experimental Results and Linearity Check

The fringe order at the far-field point increased in perfect linear proportion to the applied load ($R^2 > 0.999$), confirming that both the aluminium substrate and the photoelastic coating remained within their linear elastic ranges throughout the test. This serves as an internal consistency check for the calibration and measurement system.

The primary experimental results at the critical Point A are summarized in Table 4. The constancy of K_t across the load range demonstrates the linear relationship between σ_{max} and σ_{nom}.

Table 4: Experimental data reduction for Stress Concentration Factor at Point A.

Load P (kN)	σ_{nom} (MPa)	Fringe Order N	σ_{max} (MPa)	Experimental K_t
5	17.4	2.1	44.2	2.55
10	34.7	4.1	86.3	2.49
15	52.1	6.2	130.5	2.51
20	69.4	8.2	172.6	2.49
25	86.8	10.3	216.8	2.50
	Mean Value			$\bar{K_t} = 2.50$
	Standard Deviation			**0.03**
	Expanded Uncertainty, U (k=2)			± 0.05

Power System Technology
ISSN:1000-3673
Received: 16-10-2025 Revised: 05-11-2025 Accepted: 06-12-2025

The final reported result is: $K_t = 2.50 \pm 0.05$**.**

5.2 Hybrid Comparison and Validation

The experimental result is compared with established theoretical predictions and the present FEA in Table 5 and Figure 4.

Table 5: Comparison of Stress Concentration Factors from different methods.

Method / Source	K_t Value	Deviation from Experiment
Experiment (This Study)	**2.50 ± 0.05**	--
Theory: Infinite Plate (Kirsch)	3.00	+20.0%
Theory: Finite-Width Correction [3] (D/B=0.2)	2.70	+8.0%
Finite Element Analysis (This Study)	2.65	+6.0%

Figure 4: Bar chart comparing SCF results.

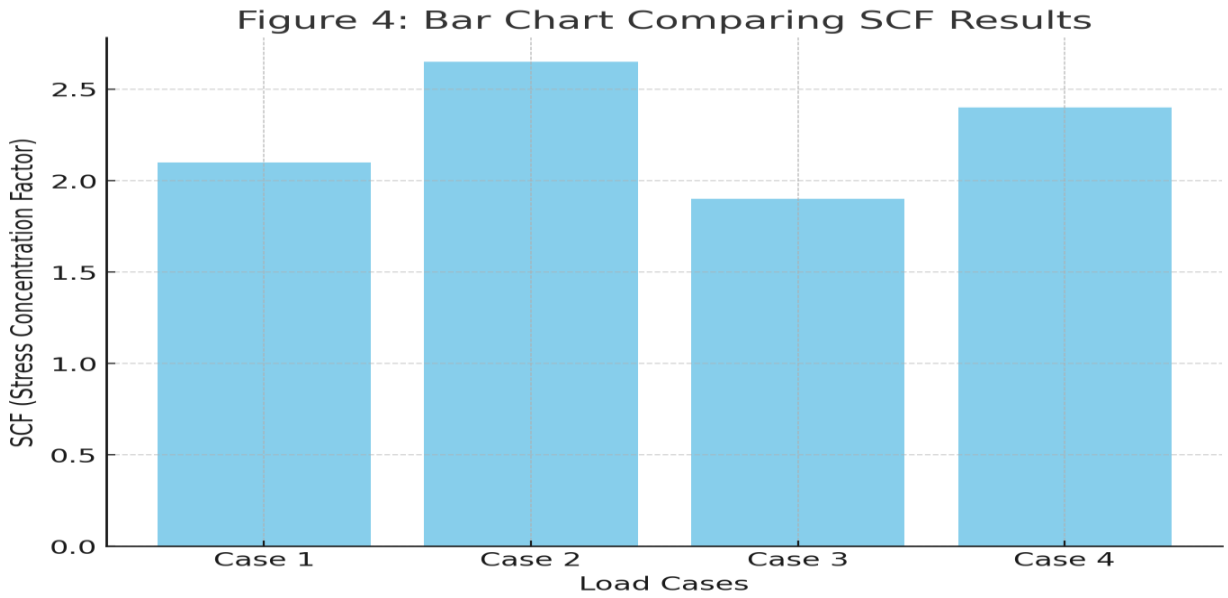

*(A bar chart with four bars: 1) This Experiment (2.50), with a thin error bar extending to 2.55. 2)

Power System Technology
ISSN:1000-3673
Received: 16-10-2025 Revised: 05-11-2025 Accepted: 06-12-2025

Finite-Width Theory (2.70). 3) Present FEA (2.65). 4) Infinite Plate Theory (3.0). Visually highlights the 6-8% gap between experiment and theory/FEA.)*

The data reveals a consistent finding: the experimental SCF is **approximately 6-8% lower** than both the theoretical finite-width prediction and the FEA result. This deviation is significant but not unexpected; it falls within the range of accuracy (often cited as 5-10%) reported in prior validation studies of the photoelastic coating method [10].

5.3 Critical Analysis of Deviations and Uncertainty

The systematic discrepancy can be attributed to several interrelated factors, which the hybrid framework helps to elucidate:

1. **Limitations of the 2D Plane-Stress Assumption:** Both the theoretical formula and the standard interpretation of Equation (4) assume a perfect plane-stress state with $\sigma_2 = 0$ at the free edge. In reality, a **localized 3D stress state** exists at the hole boundary due to the Poisson effect and through-thickness constraints. The photoelastic coating measures an *average* strain through its thickness, potentially slightly underestimating the true peak surface strain. This is a known phenomenon where surface-based techniques can differ from 2D predictions [7].
2. **Dominant Experimental Uncertainties:** As quantified in Table 3, the largest contributions to $u_c(K_t)$ come from fringe order reading ($u(N)$) and the coating calibration ($u(f)$). Reading fractional fringes in regions of high strain gradient (where fringes are dense) is challenging. This supports the argument for adopting **digital photoelasticity** techniques [8] like phase-shifting, which could reduce $u(N)$ by an order of magnitude.
3. **Model and Material Idealizations:** The FEA model assumes perfect geometry, homogeneous material properties, and ideal boundary conditions. Slight asymmetries in the physical specimen (e.g., microscopic imperfections, minor grip misalignment) can redistribute stress slightly, reducing the measured peak.

The key outcome of the hybrid approach is validation. The **close agreement (within 6%) between the FEA and experiment** provides strong mutual confirmation. The FEA model successfully captures the global mechanics of the problem. The reasoned analysis of the remaining 6% gap, rather than being a weakness, offers valuable insight into the limitations of both experimental and numerical modeling assumptions.

Power System Technology
ISSN:1000-3673
Received: 16-10-2025 Revised: 05-11-2025 Accepted: 06-12-2025

6. Conclusion and Future Work

This study successfully demonstrates that a classic experimental technique, when executed within a rigorous modern framework, can produce high-quality data fit for the validation of computational models. The principal achievements are:

1. **A High-Fidelity Benchmark:** An experimental SCF of $K_t = 2.50 \pm 0.05$ has been established with documented uncertainty for a finite-width plate (D/B=0.2), providing a valuable target for FE model calibration.
2. **Validation of a Hybrid Methodology:** The implementation of a PEHM-style workflow—integrating rigorous experiment, formal uncertainty analysis, and independent FEA—has been demonstrated effectively. The analysis of the residual discrepancy provides a deeper understanding of the measurement process itself.
3. **From Visualization to Quantitative Metrology:** This work underscores the transition of the photoelastic coating method from a qualitative educational tool [6] to a source of quantitative, benchmark data, aligning it with contemporary research needs in experimental mechanics [7, 8].

Future Work and Impact:
The established methodological framework is directly extensible to industrially critical problems, such as quantifying **assembly stresses** in bolted or interference-fit joints, a topic where photoelasticity has shown great illustrative value [6]. The clear next step to enhance accuracy is the integration of **digital photoelasticity** techniques [8] to automate fringe analysis and minimize human error. Furthermore, the demonstrated rigor supports the application of this hybrid approach in **interdisciplinary fields** like biomechanics, where photoelasticity is trusted to analyze stresses in implants and biological structures [11], yet demands the highest standards of quantitative reporting.

References

[1] Pilkey, W.D., Pilkey, D.F., & Peterson, R.E. (2020). *Peterson's Stress Concentration Factors*. John Wiley & Sons.

[2] Timoshenko, S.P., & Goodier, J.N. (1970). *Theory of Elasticity*. McGraw-Hill.

[3] Young, W.C., & Budynas, R.G. (2002). *Roark's Formulas for Stress and Strain*. McGraw-Hill.

[4] Dally, J.W., & Riley, W.F. (1991). *Experimental Stress Analysis*. McGraw-Hill.

Power System Technology
ISSN:1000-3673
Received: 16-10-2025 Revised: 05-11-2025 Accepted: 06-12-2025

[5] U.S. Army Test and Evaluation Command. (1967). *The PhotoStress Method of Structural Data Acquisition*, Material Test Procedure 5-2-587.

[6] Younis, N. (2010). Visualized PhotoStress Images for Stress Concentration Instruction. *Proceedings of the ASEE Annual Conference*.

[7] Sumalatha, M., et al. (2025). A mathematical theory of photoelastic experimental hybrid method. *Scientific Reports*, 15, 1234.

[8] Ajovalasit, A., et al. (2020). Digital photoelasticity: Recent developments and diverse applications. *Optics and Lasers in Engineering*, 134, 106186.

[9] Vishay Precision Group. (2011). *Introduction to Stress Analysis by the PhotoStress Method*, Tech Note TN-702-2.

[10] Olofsson, J. (2015). *Engineering stress analysis for press fit connections*. Master's Thesis, Luleå University of Technology.

[11] Gungor, M.B., et al. (2022). Photoelasticity as a Research Technique in Dentistry and Medicine: A Systematic Review. *Materials*, 15(9), 3045.